Langmuir

Article

pubs.acs.org/Langmuir

# High Turnover Frequency of Hydrogen Evolution Reaction on Amorphous $MoS_2$ Thin Film Directly Grown by Atomic Layer Deposition

Seokhee Shin, Zhenyu Jin, Do Hyun Kwon, Ranjith Bose, and Yo-Sep Min*

Department of Chemical Engineering, Konkuk University, 120 Neungdong-Ro, Gwangjin-Gu, Seoul 143-701, Korea

Supporting Information

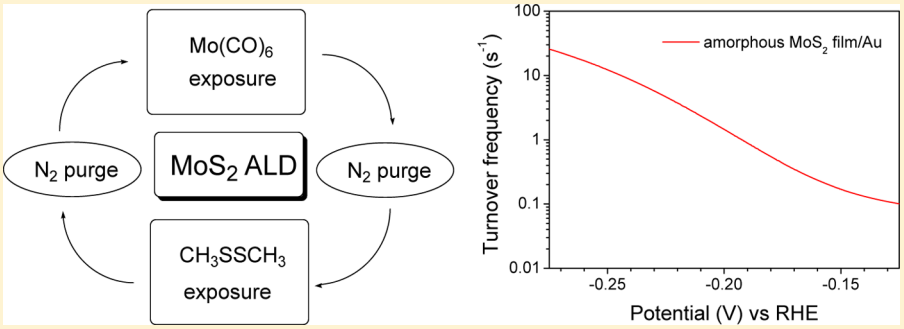


**ABSTRACT:** Recently amorphous $MoS_2$ thin film has attracted great attention as an emerging material for electrochemical hydrogen evolution reaction (HER) catalyst. Here we prepare the amorphous $MoS_2$ catalyst on Au by atomic layer deposition (ALD) using molybdenum hexacarbonyl ($Mo(CO)_6$) and dimethyl disulfide ($CH_3S_2CH_3$) as Mo and S precursors, respectively. Each active site of the amorphous $MoS_2$ film effectively catalyzes the HER with an excellent turnover frequency of 3 $H_2$/s at 0.215 V versus the reversible hydrogen electrode (RHE). The Tafel slope (47 mV/dec) on the amorphous film suggests the Volmer–Heyrovsky mechanism as a major pathway for the HER in which a primary discharging step (Volmer reaction) for hydrogen adsorption is followed by the rate-determining electrochemical desorption of hydrogen gas (Heyrovsky reaction). In addition, the amorphous $MoS_2$ thin film is electrically evaluated to be rather conductive (0.22 $\Omega^{-1}$ $cm^{-1}$ at room temperature) with a low activation energy of 0.027 eV. It is one of origins for the high catalytic activity of the amorphous $MoS_2$ catalyst.

## INTRODUCTION

$MoS_2$ is one of transition metal dichalcogenides (TMDs) which have layered two-dimensional structures. The TMD ($MX_2$), where M is a transition metal of groups 4–10 and X is a chalcogen, is one of the potential materials for electronics, Li-ion batteries, and catalysis applications.[1−3] Among them, electrocatalyst for hydrogen evolution reaction (HER, $2H^+ + 2e^- \rightarrow H_2$) has been attracted for environmentally friendly hydrogen production from water splitting.[4−8] The HER, which constitutes half of the water-splitting reaction with oxygen evolution reaction, is most efficiently catalyzed on platinum by minimizing the overpotential ($\eta$) required to drive the reduction of protons even at high reaction rates. However, Pt should be replaced with an inexpensive catalyst due to its high cost.

Widespread research has been focused on economic catalysts with high HER activity, which generally depends on Gibbs free energy of hydrogen adsorption ($\Delta G_{H^*}$).[9,10] Recently, $MoS_2$ was identified as a biomimetic catalyst for the HER, owing to a small $\Delta G_{H^*}$ on its edge sites (the hydrogen binding energy on $MoS_2$ is near to that on Pt).[11] It is well-known that only edge sites are active for the HER since the basal planes of $MoS_2$ are catalytically inert.[12−14] Thus, $MoS_2$ with exposed edges can be a promising electrocatalyst for hydrogen evolution.

Ideal HER catalysts should have low Tafel slopes ($b$) and high exchange current densities ($J_0$) as shown in the Pt catalyst ($b \sim 30$ mV/dec and $J_0 \sim 10^{-3}$ A/cm$^2$).[15] However, the bulk $MoS_2$ exhibits poor HER activity ($b \sim 692$ mV/dec) due to the lack of the exposed edge sites and the large internal resistance in the bulk semiconductor.[16] There were several approaches to expose the active edges of $MoS_2$: nanoparticles, mesoporous double-gyroid structure, vertically aligned films, and so on.[17−20] However, considering their sophisticated preparation processes, their catalytic performance is not satisfactory. Recently, Hu et al. reported that amorphous $MoS_2$ film prepared by a simple electrochemical method can achieve an excellent geometric current density of 15 mA/cm$^2$ at $\eta$ = 200 mV vs the reversible hydrogen electrode (RHE) with a Tafel slope of 40 mV/dec.[21] Since the amorphous $MoS_2$ films can be a facile approach to prepare highly active HER catalysts, here we propose a preparation method of the amorphous $MoS_2$ catalyst by atomic

Received: October 21, 2014
Revised: December 25, 2014
Published: December 29, 2014





DOI: 10.1021/la504162u
Langmuir 2015, 31, 1196–1202

layer deposition (ALD) which is well-known as a film deposition method in semiconductor industry.

ALD is one of thin film growth methods in a vacuum, in which a thin film can be deposited by a self-limiting growth mechanism via chemisorption of precursor molecules.[22] Owing to the characteristic conformal growth behavior, ALD can be utilized to prepare catalysts on a highly porous substrate.[23]

Recently, $MoS_2$ HER catalyst was prepared by sulfurizing $MoO_3$ thin film at 600 °C which was grown on glassy carbon by ALD from $Mo(CO)_6$ and ozone.[24] They obtained vertically aligned and crystallized $MoS_2$ which exhibited a geometric current density of 0.15 mA/cm$^2$ at $\eta$ = 200 mV. Loh et al. reported direct ALD of $MoS_2$ using $MoCl_5$ and $H_2S$ as Mo and S precursors, respectively.[25] However, the as-grown film was also polycrystalline due to the high growth temperature of 300 °C. Very recently, we have demonstrated a novel chemical route for ALD of $MoS_2$ using $Mo(CO)_6$ and dimethyl disulfide ($CH_3S_2CH_3$, DMDS) through which the *amorphous* $MoS_2$ film could be grown at 100 °C.[26] In this work, the HER performances of the amorphous $MoS_2$ directly grown on Au by ALD are investigated to unravel its intrinsic catalytic activity.

## EXPERIMENTAL SECTION

**Preparation and Characterization of $MoS_2$ Catalyst.** For the catalyst preparation, Ti (10 nm) and Au (100 nm) thin films were subsequently deposited on a Si wafer by sputtering, and then the wafer was cleaved to several pieces of 1 × 2 cm$^2$. The amorphous $MoS_2$ was grown at 100 °C on the Au substrate by repeating the ALD sequence: $Mo(CO)_6$ exposure (4 s)−purging (30 s)−DMDS exposure (1.5 s)−purging (10 s).[26] The geometric area (1 cm$^2$) of the $MoS_2$ catalyst was defined with a Kapton tape (see Figure S1), and then the specimen was connected to a metal wire using silver paste for the electrochemical evaluation of the HER performance.

X-ray photoelectron spectroscopic (XPS) spectra were obtained on a PHI 5000 Versaprobe (ULVAC PHI) using monochromatic Al K$\alpha$ emission. Binding energies were calibrated by using the Au $4f_{7/2}$ peak (84.0 eV). The thickness of the grown film was measured by spectroscopic ellipsometry (SE, MG-1000, NanoView). The incident angle of the polarized light in the SE was fixed at around 70°, and the incident light has a spectral range of 1.5−5.0 eV. The measured data by SE were fitted with a Tauc−Lorentz dispersion function in order to determine the thickness.[27] Scanning electron microscopic (SEM) images were taken with ultrahigh-resolution field emission SEM (Hitachi, S-5500) without any coating of metal. Grazing incidence X-ray reflectivity (XRR) data were collected in 0.01° increments and 4 s count times on a high-resolution X-ray diffractometer (Empyrean, PANalytical). XRR data were analyzed with X'pert reflectivity ver. 1.0.

**Electrochemical Characterization of $MoS_2$.** The electrochemical measurements were performed in a three-electrode electrochemical cell using a Bio-Logic potentiostat (SP-150). All measurements were performed in 100 mL of 0.5 M sulfuric acid ($H_2SO_4$) electrolyte prepared in Millipore water (18 MΩ cm) purged with $H_2$ gas (99.999%). A $Hg/Hg_2SO_4$ ($K_2SO_4$ saturated) electrode and a graphite rod were used as a reference electrode and a counter electrode, respectively. The $MoS_2$ film prepared on Au was used as a working electrode. The reference electrode was calibrated to the reversible hydrogen potential using Pt wires for both working and counter electrodes in the same 0.5 M $H_2SO_4$ electrolyte under the $H_2$ gas purge. This calibration gives a shift of −0.700 ± 0.005 V versus the RHE. The polarization curves for the HER were measured using linear sweep voltammetry (LSV) beginning at 0.1 V and ending at −0.3 V vs RHE with a scan rate of 5 mV/s. Before each LSV, the series resistance of the electrochemical cell was determined by electrochemical impedance measurement performed at open circuit potential from 200 kHz to 50 mHz, using an ac amplitude of 25 mV. The series resistance was measured to be ∼2.5 Ω, and the polarization curves were corrected for the ohmic potential drop ($iR$) losses (see Figure S2). In order to estimate the effective surface area of the catalyst film, the double-layer capacitance ($C_{dl}$) of the catalyst were determined by cyclic voltammetry in a potential range of 0.1−0.2 V with various scan rates (20, 40, 60, 80, and 100 mV/s; see Figure S3).

**Electrical Characterization of $MoS_2$.** In order to evaluate electrical conductivity, ALD $MoS_2$ thin film (12.7 nm) was grown on $SiO_2$ (300 nm)/Si substrate at 100 °C. Coplanar Au electrodes were formed on the surface of the film by thermal evaporation through a shadow mask. The distance between the neighboring electrodes was 400 $\mu$m, and the width of each electrode was 400 $\mu$m. Current−voltage characteristic measurements were performed at a temperature range of 110−300 K between the neighboring two electrodes in a vacuum probe station (MS-Tech M5VC) using a semiconductor parameter analyzer (Keithley 4200 SCE).

## RESULTS AND DISCUSSION

**Characterization of Amorphous $MoS_2$ Catalyst.** In Figure 1, the ALD $MoS_2$ film on Au is characterized by XPS.

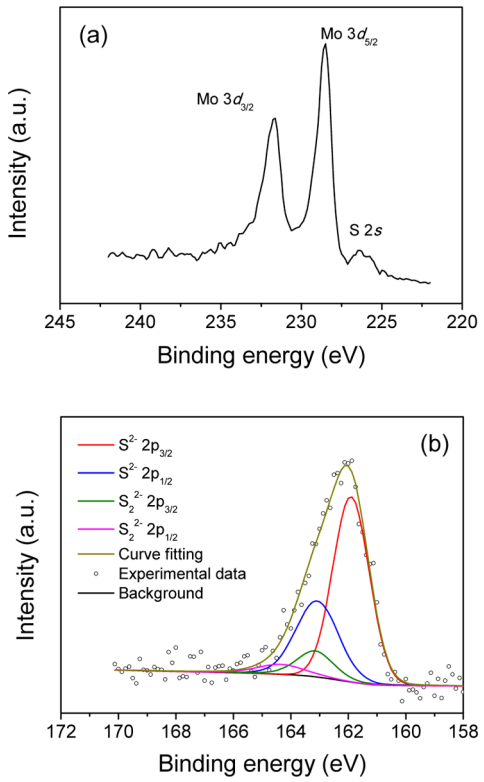


**Figure 1.** XPS spectra of $MoS_2$ film on Au: Mo 3d (a) and S 2p (b) peaks. The binding energies were calibrated by using the Au $4f_{7/2}$ peak (84.0 eV). The curve fitting was performed with two constraints: the intensity ratio (1:2) and the binding energy difference (1.18 eV) of S $2p_{1/2}$ and $2p_{3/2}$ for both $S^{2-}$ and $S_2^{2-}$ ions.

The characteristic binding energies of Mo $3d_{3/2}$ and $3d_{5/2}$, which are attributed to $Mo^{4+}$, were observed at 231.6 and 228.5 eV, respectively.[21,28−30] For the binding energies of S $2p_{1/2}$ and $2p_{3/2}$ for divalent sulfide ion ($S^{2-}$), the $2p_{3/2}$ peak was observed at 162.0 eV. However, the $2p_{1/2}$ peak is not clearly resolved but may be hidden as a shoulder of the $2p_{3/2}$ peak. The stoichiometric ratio (S/Mo), estimated from peak intensities on the surface, is around 2.19, suggesting that the film is close to $MoS_2$. The slightly higher stoichiometric ratio can be explained by the presence of $MoS_3$ in the film. Several groups reported the amorphous $MoS_3$ thin film which corresponds to a formal charge state of $Mo^{4+}(S^{2-})(S_2^{2-})$.[21,28,29,31]



DOI: 10.1021/la504162u
Langmuir 2015, 31, 1196−1202

It is well-known that the peaks of S $2p_{1/2}$ and $2p_{3/2}$ for $S_2^{2-}$ appear at higher binding energies than those of $S^{2-}$. In order to confirm the presence of the $S_2^{2-}$ ion, the S 2p spectrum in Figure 1 was deconvoluted and fitted with two doublets, i.e., $2p_{3/2}$ (161.9 eV) and $2p_{1/2}$ (163.1 eV) for the $S^{2-}$ and $2p_{3/2}$ (163.2 eV) and $2p_{1/2}$ (164.4 eV) for the $S_2^{2-}$ ion.[21,29] The ratio of $S^{2-}$ to $S_2^{2-}$ was evaluated to be ~6.4 using the intensities of the doublets. By using the ratio of S ions, the stoichiometric ratio (S/Mo) can be calculated to be ~2.27, which agrees well with the measured value (~2.19).

When our ALD process was performed on $SiO_2$/Si substrate in the previous report,[26] although the as-grown film was amorphous in X-ray diffraction, the film clearly showed two characteristic Raman modes of $E^1_{2g}$ and $A_{1g}$ associated with in-plane and out-of-plane vibrational modes of S−Mo−S, respectively.[32,33] Unlike the amorphous films grown on $SiO_2$/Si substrates, no significant peaks of the $E^1_{2g}$ and $A_{1g}$ modes were observed from the amorphous $MoS_2$/Au specimen (data not shown). This indicates that the grown film is even more disordered on Au than on $SiO_2$/Si substrate.

**Hydrogen Evolution Catalysis on Amorphous $MoS_2$ Thin Film.** The amorphous films on Au were used as a working electrode for hydrogen evolution in 0.5 M $H_2SO_4$ solution using a typical three-electrode setup. Figure 2 shows polarization curves of two $MoS_2$ films with different thicknesses (2.0 and 9.4 nm, measured by SE) and a bare Au specimen as a control sample. Each curve was corrected for ohmic potential drop ($iR$) losses (see Figure S2). Comparing to the cathodic current density ($j$) of Au specimen ($j$ = 62 $\mu$A/cm$^2$ at $\eta$ = 200 mV), the amorphous $MoS_2$ films show much higher current densities at lower overpotential. In addition, the thicker film ($j$ = 532 $\mu$A/cm$^2$ at $\eta$ = 200 mV) shows better activity than the thinner ($j$ = 241 $\mu$A/cm$^2$ at $\eta$ = 200 mV). The high catalytic activity of the ALD-$MoS_2$ is more obvious when compared with the onset potential at which the hydrogen evolution starts. Because it is difficult to visually recognize the initiation of the hydrogen evolution, the onset potential is defined as the overpotential required for a designated current density of 100 $\mu$A/cm$^2$. Comparing to the onset potential (222 mV) of the bare Au in Figure 2, the thick and thin $MoS_2$ films show much smaller onset potentials of 165 and 181 mV, respectively, which are well agreed with the previous reports.[8]

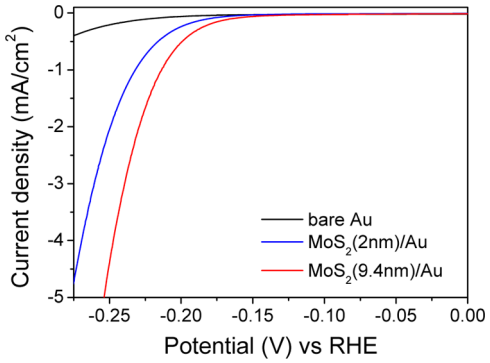


**Figure 2.** Polarization curves ($iR$-corrected) of $MoS_2$ films measured in an aqueous solution of $H_2SO_4$ (0.5 M) with a scan rate of 5 mV/s.

The electrode kinetics in electrochemical reactions can be explained by the Butler−Volmer equation.[34] Under the assumption of no mass-transfer effect, the equation can be simplified to

$$j = j_0[e^{(1-\beta)\eta F/RT} - e^{-\beta\eta F/RT}] \quad (1)$$

where $F$ and $R$ are the Faraday constant and gas constant, respectively, and $\beta$ is the symmetry factor ($\beta \sim 0.5$) which is an indicator of the symmetry of the energy barrier for the reaction. The exchange current density ($j_0$) is a quantitative measure of the rate of reaction at equilibrium (i.e., $\eta$ = 0). When the overpotential is largely negative as the linear portion of the polarization curve in Figure 2, the current density can be approximated only with the second term (cathodic current density), which is called the Tafel equation:

$$j = -j_0 e^{-\beta\eta F/RT} \quad (2)$$

The figures of merit for electrocatalytic activity can be obtained from the slope and the intercept in the log $j$ axis by fitting the linear potion of the polarization curve to the semilogarithmic equation of $\eta = a + b \log j$. Table 1 summarizes the Tafel slopes ($b$) and $j_0$ values obtained from the Tafel plots in Figure 3.

**Table 1. Figures of Merit for Electrocatalytic Activity of $MoS_2$ Films**

| samples | Tafel slope (mV/dec) | $J_0$ ($\mu$A/cm$^2$) | onset potential (V) | TOF at 0.2 V vs RHE ($H_2$/s) |
|---|---|---|---|---|
| bare Au | 88 | 0.293 | −0.222 | |
| $MoS_2$ (2.0 nm) | 50 | 0.024 | −0.181 | |
| $MoS_2$ (9.4 nm) | 47 | 0.027 | −0.165 | 1.45 |

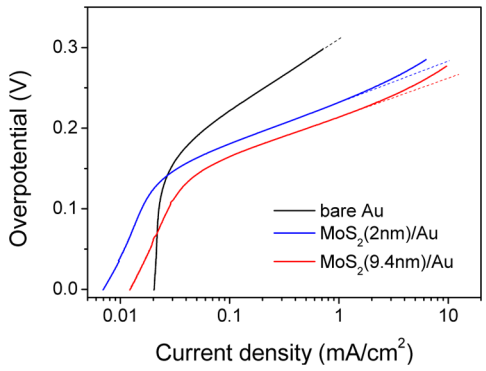


**Figure 3.** Tafel plots of $MoS_2$ films measured in an aqueous solution of $H_2SO_4$ (0.5 M) with a scan rate of 5 mV/s. The dotted lines are drawn for an eye guide of the Tafel slopes.

For the bare Au specimen, the exchange current density is 0.293 $\mu$A/cm$^2$, which agrees well with the values ranged in the $10^{-8}$−$10^{-7}$ A/cm$^2$ in the previous reports.[4,12,35,36] The $J_0$ values of $MoS_2$ films are about 1 order of magnitude lower than that of the bare Au. However, since the $MoS_2$ films have much smaller Tafel slopes (47−50 mV/dec) than that (88 mV/dec) of Au, they show more excellent HER activity in Figure 2.

According to the classical theory on the HER kinetics, the Tafel slope is determined by the transfer coefficient ($\alpha$) which has a particular value depending on the mechanism.[37]

$$b = \frac{\partial\eta}{\partial \log j} = -\frac{RT}{\alpha F} \ln e \quad (3)$$

Three possible reaction steps are known for the HER in acidic media:



DOI: 10.1021/la504162u
Langmuir 2015, 31, 1196−1202

discharge step (Volmer reaction):

$$H_3O^+ + e^- \rightarrow H_{ads} + H_2O \quad (4)$$

catalytic recombination step (Tafel reaction):

$$H_{ads} + H_{ads} \rightarrow H_2 \quad (5)$$

electrochemical desorption step (Heyrovsky reaction):

$$H_{ads} + H_3O^+ + e^- \rightarrow H_2 + H_2O \quad (6)$$

For hydrogen evolution, there are two possible pathways: Volmer−Tafel (VT) and Volmer−Heyrovsky (VH) mechanisms. Furthermore, the transfer coefficient is different depending on which step is the rate-determining step (rds). For the Volmer (rds)−Tafel mechanism ($\bar{V}T$, the bar denotes the rds), in which the rate-determining Volmer step is followed by the Tafel step, $\alpha = \beta = 0.5$, and this mechanism has a Tafel slope of 120 mV/dec by eq 3. However, when the Tafel step is the rds, the $V\bar{T}$ mechanism has a Tafel slope of 30 mV/dec ($\alpha = 2$ and $\beta = 0.5$). For the VH mechanism, the Tafel slopes are 120 mV/dec for the $\bar{V}H$ mechanism ($\alpha = \beta = 0.5$) and 40 mV/dec for the $V\bar{H}$ mechanism ($\alpha = 1.5$ and $\beta = 0.5$).

Considering the Tafel slopes ($b$ = 47 mV/dec) from the amorphous $MoS_2$ films, the $V\bar{H}$ mechanism might be the main pathway for the HER on our catalyst. Several groups also reported similar Tafel slopes from various forms of $MoS_2$: nanoparticles on reduced graphene (40 mV/dec),[17] electrochemically grown film on glassy carbon (41 mV/dec),[21] amorphous film on nanoporous gold (41 mV/dec),[36] vertically aligned film (44 mV/dec),[24] double-gyroid network (50 mV/dec),[18] and nanocrystals on gold (55−60 mV/dec).[12] However, the deviation of the Tafel slope from the theoretical value (40 mV/dec) of the $V\bar{H}$ mechanism reveals that other reaction pathway partially contributes to the reaction. Previously, it is reported that a Tafel slope of 60 mV/dec can be obtained when a chemical rearrangement step is inserted as a rds between the Volmer and Heyrovsky steps.[14,38] If proton adsorption is much stronger on a certain type of active sites than on others, the strongly adsorbed $H_{ads}$ will not be able to easily reach a necessary condition for the Heyrovsky step. Therefore, the surface rearrangement of $H_{ads}$ would be rate-determining. Because of significant heterogeneity of the surface sites or the presence of both $S^{2-}$ and $S_2^{2-}$ in the amorphous $MoS_2$ catalyst, it would be possible that some active sites might bind the surface hydrogen more strongly than the other.

Even though the $j_0$ is an inherent measure of activity for the HER, it is sometimes unfair to compare the activities of catalysts with the $j_0$ values since the geometric area of catalyst can be largely different from a catalytically effective surface area due to their surface roughness or porosity. In this point of view, turnover frequency (TOF) per active site, which is defined as the number of hydrogen molecules evolved on an active site in a time period (e.g., in 1 s), is the best figure of merit to compare the catalytic activity.[14,39] Assuming the cathodic current is entirely attributed to the HER, the TOF can be calculated from the $j$ (e.g., in A/cm$^2$) by using an equation of TOF = $j/nFN$ with a known value of number of active sites ($N$) in an unit area (e.g., in cm$^2$) where $n$ is the stoichiometric number of electrons consumed in the electrode reaction (i.e., $n$ = 2 for the HER). Because of the different nature of various $MoS_2$ catalysts and their preparation methods, several approaches have been used to determine the $N$ values (see the Supporting Information of ref 14). Because our ALD-grown film is amorphous, the structure and properties of $MoS_2$ can be assumed to be isotropic. Therefore, the $N$ value may be estimated from the amorphous film density ($d$) by

$$N = R_f(N_A d/M_f)^{2/3} \quad (7)$$

where $N_A$ and $M_f$ are Avogadro's number and formula weight of $MoS_2$, respectively, and $R_f$ is a surface roughness factor defined as a ratio of the real surface area to the geometric area.

In this work, the film density ($d$) of the amorphous $MoS_2$ was determined by grazing incidence X-ray reflectivity (XRR, Figure S4). The measured density (~2.9 g/cm$^3$) of the amorphous film, grown at 100 °C, is much lower than that (5.06 g/cm$^3$) of crystalline $MoS_2$.[40] In general, as amorphous films are grown at lower temperatures by ALD, they have lower density.[41] Assuming a flat $MoS_2$ ($R_f \sim 1$), the number of active sites on the flat surface of the amorphous $MoS_2$ is approximately calculated to be ~4.9 × 10$^{14}$/cm$^2$ by eq 7. Because of the low density of the amorphous film, this value is roughly a factor of 2 lower than the number of active sites (1.164 × 10$^{15}$/cm$^2$) on a flat surface of crystalline $MoS_2$.[42] However, as shown in SEM images in Figure S5, the surface of the amorphous films is not flat because the film was grown on Au with crystalline grains. Thus, $R_f \neq 1$ and the roughness factor should be considered when calculating the $N$ value. The $R_f$ of the amorphous film was determined by the ratio of double layer capacitance ($C_{dl}$) of the amorphous $MoS_2$ to that (66.7 $\mu$F/cm$^2$) of flat crystalline $MoS_2$,[43] since the $C_{dl}$ is linearly proportional to catalytically active surface area.[44] It is assumed that the $C_{dl}$ values of amorphous film and the crystalline $MoS_2$ are the same in the case of flat surfaces. The $C_{dl}$ value of the amorphous film (9.4 nm) was estimated to be ~152 $\mu$F/cm$^2$ by cyclic voltammetry (see Figure S3). Therefore, the roughness factor of the film is ~2.28, and the $N$ value is around 1.12 × 10$^{15}$/cm$^2$ by eq 7.

The TOF (per active site) can be calculated by using the equation of TOF = $j/nFN$, where $N$ = 1.12 × 10$^{15}$/cm$^2$. The TOF of the amorphous $MoS_2$ (9.4 nm)/Au catalyst is shown in Figure 4 within the Tafel region in order to guarantee that the HER is controlled by electrode kinetics without any other effect (e.g., mass transfer). In terms of the TOF per active site, the most active catalyst of $MoS_2$ is vacuum-deposited nanocrystals on Au, of which TOFs are 1 and 10 $H_2$/s at overpotentials of ~0.1 and ~0.16 V, respectively.[12] The same TOFs can be achieved on our amorphous film at overpotentials of 0.193 and 0.244 V, respectively. Even though the amorphous $MoS_2$ shows lower TOFs than the nanocrystals, the intrinsic activity (e.g.,

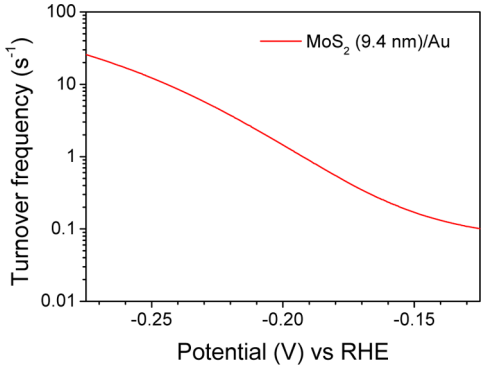


**Figure 4.** Turnover frequency (TOF) of amorphous $MoS_2$ film (9.4 nm)/Au.



DOI: 10.1021/la504162u
Langmuir 2015, 31, 1196−1202

TOF = 3 $H_2$/s at 0.215 V and 1.45 $H_2$/s at 0.2 V) of the ALD-$MoS_2$ is comparable to that of crystalline thiomolybdate cluster catalyst which has the second highest TOF (3 $H_2$/s at an overpotential of 0.20 V) among all molybdenum sulfide catalysts ever reported.[14] Furthermore, our ALD-$MoS_2$ has the highest TOF among those of the amorphous $MoS_x$ ever reported. For example, comparing to the TOF (e.g., TOF = 0.8 $H_2$/s at 0.22 V and 2 $H_2$/s at 0.24 V) of the amorphous $MoS_x$ film grown by cyclic voltammetric method,[21] our catalyst shows 4 times higher TOF (per active site) at the same overpotential (i.e., TOF = 3.7 $H_2$/s at 0.22 V and 8.5 $H_2$/s at 0.24 V). This high TOF is the biggest advantage of the ALD-$MoS_2$ catalyst for the HER. Although the exchange current density of the ALD-$MoS_2$ is not high due to the lower roughness factor in comparison to the other forms of $MoS_2$, it may be overcome by using porous substrates with large surface area. Furthermore, the ALD is one of the best methods when forming a conformal film on a porous substrate.[23]

The stability of a HER catalyst is another practical parameter to consider when designing long-term operations. A cyclic voltammetry test for 1000 cycles was performed to assess the electrochemical stability of the ALD-$MoS_2$ in an acidic environment (0.5 M $H_2SO_4$). Unfortunately, the amorphous ALD-$MoS_2$ on Au shows poor stability (Figure S6). There are many reports for the excellent stability of the *crystalline* $MoS_2$ on various substrates such as Au, graphene, and glassy carbon.[17,19,24] However, the good stability of the *amorphous* $MoS_2$ is very rarely reported. It is recently studied that the factors contributing to the activity loss of the amorphous $MoS_2$ may be due to the surface adsorbates, which can poison the active sites, or delamination of $MoS_2$ from the substrate.[42] Sun et al. also demonstrated that the catalytic stability could be excellent when the amorphous $MoS_2$ was prepared on Mo foil by an in-situ fabrication approach to avoid the delarmination.[45] However, to the extent of our knowledge, no reports were made on excellent stability of the amorphous $MoS_2$/Au catalyst, which could possibly be due to the poor adhesion of the $MoS_2$ on Au. Therefore, it is necessary to replace Au with cheap and porous substrates (e.g., carbon fiber paper) which can provide a surface for strong adhesion of amorphous $MoS_2$. Substrate-related issues are beyond the scope of this work, and further study will be presented elsewhere.

**Electrical Conductivity of Amorphous $MoS_2$ Thin Film.** One more concern for the amorphous $MoS_2$ is the electrical conductivity ($\sigma$) of the film. The crystalline bulk $MoS_2$ has a poor catalytic activity due to the large internal resistance, especially in the direction perpendicular to the $MoS_2$ layers. The electrical conductivity of crystalline $MoS_2$ is extremely anisotropic so that the conductivity ($10^{-5}$–$10^{-4}$ $\Omega^{-1}$ $cm^{-1}$) perpendicular to the layers is approximately 3 orders of magnitude smaller than that ($10^{-2}$–$10^{-1}$ $\Omega^{-1}cm^{-1}$) parallel to the layer.[16,46,47] In Figure 5, the conductivity of the amorphous film was evaluated at a temperature range of 110–300 K by using a simple two-probe measurement setup between two coplanar Au electrodes on the film surface. The conductivity of the film is around 0.22 ± 0.02 $\Omega^{-1}$ $cm^{-1}$ at room temperature. This value is similar to or slightly higher than the conductivity parallel to the layer of the bulk.[46]

In addition, the conductivity of the amorphous film logarithmically increases with temperature due to the semiconducting nature. Such a thermally activated conductivity can be represented by the Boltzmann law:

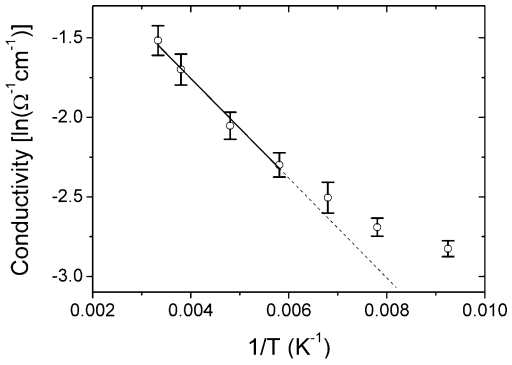


**Figure 5.** Arrhenius plot of conductivity of amorphous $MoS_2$ thin film. It was measured between two coplanar surface electrodes (Au) on $MoS_2$ (10 nm)/$SiO_2$ (300 nm)/Si substrate.

$$\sigma = \sigma_0 e^{-E_a/kT} \quad (8)$$

where $E_a$ and $k$ are the activation energy and the Boltzmann constant, respectively. Using the slope of the Arrhenius plot in a range of 170–300 K in Figure 5, we determined the activation energy to be ~0.027 ± 0.004 eV, which is similar to or lower than the activation energy (0.03–0.08 eV) for the conduction parallel to the layer in the bulk.[48,49] The deviation from the linearity at lower temperatures than 150 K can be explained with hopping of electrons through localized states which becomes dominant at lower temperatures.[48] Consequently, another reason for the high catalytic activity of the amorphous film would be its isotropic high conductivity with a low activation energy.

## ■ CONCLUSIONS

For facile preparation of amorphous $MoS_2$ catalyst, we utilize direct growth of amorphous $MoS_2$ by ALD using $Mo(CO)_6$ and DMDS. The amorphous $MoS_2$ thin film exhibits excellent HER activity with a high TOF (3 $H_2$/s at an overpotential of 0.215 V) per active site. This is the highest TOF reported to date for amorphous $MoS_2$ catalyst. The Tafel slope of 47 mV/dec reveals that the HER on the amorphous film is catalyzed via the Volmer–Heyrovsky mechanism of which the rate-determining step is the electrochemical desorption of hydrogen. In addition, the amorphous $MoS_2$ has an electrical conductivity of 0.22 ± 0.02 $\Omega^{-1}$ $cm^{-1}$ at room temperature with an activation energy of 0.027 ± 0.004 eV.

## ■ ASSOCIATED CONTENT

### Supporting Information

Digital image of $MoS_2$ catalyst specimen, correction of ohmic potential drop, SEM images, XRR data, double-layer capacitance, electrochemical impedance measurements, and stability test. This material is available free of charge via the Internet at http://pubs.acs.org.

## ■ AUTHOR INFORMATION

### Corresponding Author

*E-mail: ysmin@konkuk.ac.kr (Y.-S.M.).

### Author Contributions

S.S. and Z.J. equally contributed to this work.

### Notes

The authors declare no competing financial interest.



DOI: 10.1021/la504162u
*Langmuir* 2015, 31, 1196–1202

## ■ ACKNOWLEDGMENTS

This work (Grant C0147404) was supported by Business for Cooperative R&D between Industry, Academy, and Research Institute funded by Korea Small and Medium Business Administration in 2013. This research was also partially supported by Basic Science Research Program through the National Research Foundation of Korea which is funded by the Ministry of Education (NRF-2014R1A1A2055812). The authors also thank H. K. Kang (Advanced Analysis Center, KIST) for XPS analysis.

## ■ REFERENCES

(1) Chhowalla, M.; Shin, H. S.; Eda, G.; Li, L. J.; Loh, K. P.; Zhang, H. The Chemistry of Two-Dimensional Layered Transition Metal Dichalcogenide Nanosheets. *Nat. Chem.* **2013**, *5*, 263−275.

(2) Huang, X.; Zeng, Z.; Zhang, H. Metal Dichalcogenide Nanosheet: Preparation, Properties and Applications. *Chem. Soc. Rev.* **2013**, *42*, 1934−1946.

(3) Wang, Q. H.; Kalantar-Zadeh, K.; Kis, A.; Coleman, J. N.; Strano, M. S. Electronics and Optoelectronics of Two-Dimensional Transition Metal Dichalcogenides. *Nat. Nanotechnol.* **2012**, *7*, 699−712.

(4) Kibler, L. A. Hydrogen Electrocatalysis. *ChemPhysChem* **2006**, *7*, 985−991.

(5) Laursen, A. B.; Kegns, S.; Dahl, S.; Chorkendorff, I. Molybdenum Sulfide − Efficient and Viable Materials for Electro- and Photoelectrocatalytic Hydrogen Evolution. *Energy Environ. Sci.* **2012**, *5*, 5577−5591.

(6) Morales-Guio, C. G.; Stern, L. A.; Hu, X. Nanostructured Hydrotreating Catalysts for Electrochemical Hydrogen Evolution. *Chem. Soc. Rev.* **2014**, *43*, 6555−6569.

(7) Yan, Y.; Xia, B.; Xu, Z.; Wang, X. Recent Development of Molybdenum Sulfide as Advanced Electrocatalysts for Hydrogen Evolution Reaction. *ACS Catal.* **2014**, *4*, 1693−1705.

(8) Yang, J.; Shin, H. S. Recent Advances in Layered Transition Metal Dichalcogenides for Hydrogen Evolution Reaction. *J. Mater. Chem. A* **2014**, *2*, 5979−5986.

(9) Conway, B. E.; Bockris, J. O. M. Electrolyitc Hydrogen Evolution Kinetics and Its Relation to the Electronic and Adsorptive Properties of the Metal. *J. Chem. Phys.* **1957**, *26*, 532−541.

(10) Norskov, J. K.; Bligaard, T.; Rossmeisl, J.; Christensen, C. H. Towards the Computational Design of Solid Catalysts. *Nat. Chem.* **2009**, *1*, 37−46.

(11) Hinnemann, B.; Moses, P. G.; Bonde, J.; Jorgensen, K. P.; Nielsen, J. H.; Horch, S.; Chorkendorff, I. B.; Norskov, J. K. Biomimetic Hydrogen Evolution: $MoS_2$ Nanoparticles as Catalyst for Hydrogen Evolution. *J. Am. Chem. Soc.* **2005**, *127*, 5308−5309.

(12) Jaramillo, T. F.; Jorgensen, K. P.; Bonde, J.; Nielsen, J. H.; Horch, S.; Chorkendorff, I. Identification of Active Edge Sites for Electrochemical $H_2$ Evolution from $MoS_2$ Nanocatalysts. *Science* **2007**, *317*, 100−102.

(13) Karunadasa, H. I.; Montalvo, E.; Sun, Y.; Majda, M.; Long, J. R.; Chang, C. J. A Molecular $MoS_2$ Edge Site Mimic for Catalytic Hydrogen Generation. *Science* **2012**, *335*, 698−702.

(14) Kibsgaard, J.; Jaramillo, T. F.; Besenbacher, F. Building an Appropriate Acitve-Site Motif into a Hydrogen-Evolution Catalyst with Thiomolybdate $[Mo_3S_{13}]^{2-}$ Clusters. *Nat. Chem.* **2014**, *6*, 248−253.

(15) Conway, B. E.; Tilak, B. V. Interfacial Processes Involving Electrocatalytic Evolution and Oxidation of $H_2$, and the Role of Chemisorbed H. *Electrochim. Acta* **2002**, *47*, 3571−3594.

(16) Tributsch, H.; Bennett, J. C. Electrochemistry and Photochemistry of $MoS_2$ Layer Crystals. I. *J. Electroanal. Chem.* **1977**, *81*, 97−111.

(17) Li, Y.; Wang, H.; Xie, W. L.; Liang, Y.; Hong, G.; Dai, H. $MoS_2$ Nanoparticles Grown on Graphene: an Advanced Catalyst for the Hydrogen Evolution Reaction. *J. Am. Chem. Soc.* **2011**, *133*, 7296−7298.

(18) Kibsgaard, J.; Chen, Z.; Reinecke, B. N.; Jaramillo, T. F. Engineering the Surface Structure of $MoS_2$ to Preferentially Expose Active Edge Sites for Electrocatalysis. *Nat. Mater.* **2012**, *11*, 963−969.

(19) Wang, T.; Liu, L.; Zhu, Z.; Papakonstantinou, P.; Hu, J.; Liu, H.; Li, M. Enhanced Electrocatalytic Activity for Hydrogen Evolution Reaction from Self-Assembled Monodispersed Molybdenum Sulfide Nanoparticles on an Au Electrode. *Energy Environ. Sci.* **2013**, *6*, 625−633.

(20) Kong, D.; Wang, H.; Cha, J. J.; Pasta, M.; Koshi, K. J.; Yao, J.; Cui, Y. Synthesis of $MoS_2$ and $MoSe_2$ Films with Vertically Aligned Layers. *Nano Lett.* **2013**, *13*, 1341−1347.

(21) Merki, D.; Fierro, S.; Vrubel, H.; Hu, X. Amorphous Molybdenum Sulfide Films as Catalysts for Electrochemical Hydrogen Production in Water. *Chem. Sci.* **2011**, *2*, 1262−1267.

(22) George, S. M. Atomic Layer Deposition: an Overview. *Chem. Rev.* **2010**, *110*, 111−131.

(23) Lee, H. Y.; An, C. J.; Piao, S. J.; Ahn, D. Y.; Kim, M. T.; Min, Y. S. Shrinking Core Model for Knudsen Diffusion-Limited Atomic Layer Deposition on a Nanoporous Monolith with an Ultrahigh Aspect Ratio. *J. Phys. Chem. C* **2010**, *114*, 18601−18606.

(24) Wang, H.; Lu, Z.; Xu, S.; Kong, D.; Cha, J. J.; Zheng, G.; Hsu, P. C.; Yan, K.; Bradshaw, D.; Prinz, F. B.; Cui, Y. Electrochemical Tuning of Vertically Aligned $MoS_2$ Nanofilms and Its Application in Improving Hydrogen Evolution Reaction. *Proc. Natl. Acad. Sci. U. S. A.* **2013**, *110*, 19701−19706.

(25) Tan, L. K.; Liu, B.; Teng, J. H.; Guo, S.; Low, H. Y.; Loh, K. P. Atomic Layer Deposition of $MoS_2$ Film. *Nanoscale* **2014**, *6*, 10584−10588.

(26) Jin, Z.; Shin, S.; Kwon, D. H.; Han, S. J.; Min, Y. S. Novel Chemical Route for Atomic Layer Deposition of $MoS_2$ Thin Film on $SiO_2$/Si Substrate. *Nanoscale* **2014**, *6*, 14453−14458.

(27) Yim, C.; O'Brien, M.; McEvoy, N.; Winters, S.; Mirza, I.; Lunney, J. G.; Duesberg, G. S. Investigation of the Optical Properties of $MoS_2$ Thin Films Using Spectroscopic Ellipsometry. *Appl. Phys. Lett.* **2014**, *104*, 103114-1−113114-5.

(28) McDevitt, N. T.; Bultman, J. E.; Zabinski, J. S. Study of Amorphous $MoS_2$ Films Grown by Pulsed Laser Deposition. *Appl. Spectrosc.* **1998**, *52*, 1160−1164.

(29) Chang, Y. H.; Lin, C. T.; Chen, T. Y.; Hsu, C. L.; Lee, Y. H.; Zhang, W. Z.; Wei, K. H.; Li, L. J. Highly Efficient Electrocatalytic Hydrogen Production by $MoS_x$ Grown on Graphene-Protected 3D Ni Foams. *Adv. Mater.* **2013**, *25*, 756−760.

(30) Baker, M. A.; Gilmore, R.; Lenardi, C.; Gissler, W. XPS Investigation of Preferential Sputtering of S from $MoS_2$ and Determination of $MoS_x$ Stoichiometry from Mo and S Peak Positions. *Appl. Surf. Sci.* **1999**, *150*, 255−262.

(31) Weber, T.; Muijsers, J. C.; Niemantsverdriet, J. W. Structure of Amorphous $MoS_3$. *J. Phys. Chem.* **1995**, *99*, 9194−9200.

(32) Verble, J. L.; Wieting, T. J. Lattice Mode Degeneracy in $MoS_2$ and Other Layer Compounds. *Phys. Rev. Lett.* **1970**, *25*, 362.

(33) Lee, C.; Yan, H.; Brus, L. E.; Heinz, T. F.; Hone, J.; Ryu, S. Anomalous Lattice Vibrations of Single- and Few-Layer $MoS_2$. *ACS Nano* **2010**, *4*, 2695−2700.

(34) Bard, A. J.; Faulkner, L. R. *Electrochemical Method: Fundamentals and Applications*, 2nd ed.; Wiley: New York, 2001; p 100.

(35) Norskov, J. K.; Bligaard, T.; Logadottir, A.; Kitchin, J. R.; Chen, J. G.; Pandelov, S.; Stimming, U. Trends in the Exchange Current for Hydrogen Evolution. *J. Electrochem. Soc.* **2005**, *152*, J23−J26.

(36) Ge, X.; Chen, L.; Zhang, L.; Wen, Y.; Hirata, A.; Chen, M. Nanoporous Metal Enhanced Catalytic Activities of Amorphous Molybdenum Sulfide for High-Efficiency Hydrogen Production. *Adv. Mater.* **2014**, *26*, 3100−3104.

(37) Bockris, J. O. M.; Reddy, A. K. N. *Modern Electrochemistry*, 1st ed.; Plenum Press: New York, 1970; p 1242.

(38) Kodintsev, I. M.; Trasatti, S. Electrocatalysis of $H_2$ Evolution on $RuO_2$ + $IrO_2$ Mixed Oxide Electrodes. *Electrochim. Acta* **1994**, *39*, 1803−1808.

(39) Boudart, M. Turnover Rates in Heterogeneous Catalysis. *Chem. Rev.* **1995**, *95*, 661−666.



DOI: 10.1021/la504162u
*Langmuir* 2015, 31, 1196−1202

(40) Lide, D. R. *Handbook of Chemistry and Physics*, 86th ed.; CRC Press: Boca Raton, FL, 2005; pp 4−74.
(41) Groner, M. D.; Fabreguette, F. H.; Elam, J. W.; George, S. M. Low-Temperature $Al_2O_3$ Atomic Layer Deposition. *Chem. Mater.* **2004**, *16*, 639−645.
(42) Benck, J. D.; Chen, Z.; Kuritzky, L. Y.; Forman, A. J.; Jaramillo, T. F. Amorphous Molybdenum Sulfide Catalysts for Electrochemical Hydrogen Production: Insights into the Origin of their Catalytic Activity. *ACS Catal.* **2012**, *2*, 1916−1923.
(43) Yu, Y.; Huang, S. Y.; Li, Y.; Steinmann, S.; Yang, W.; Cao, L. Layer-Dependent Electrocatalysis of $MoS_2$ for Hydrogen Evolution. *Nano Lett.* **2014**, *14*, 553−558.
(44) Lukowski, M. A.; Daniel, A. S.; Meng, F.; Forticaux, A.; Li, L.; Jin, S. Enhanced Hydrogen Evolution Catalysis from Chemically Exfoliated Metallic $MoS_2$ Nanosheets. *J. Am. Chem. Soc.* **2013**, *135*, 10274−10277.
(45) Lu, Z.; Zhang, H.; Zhu, W.; Yu, X.; Kuang, Y.; Chang, Z.; Lei, X.; Sun, X. In Situ Fabrication of Porous $MoS_2$ Thin-Films as High-Performance Catalysts for Electrochemical Hydrogen Evolution. *Chem. Commun.* **2013**, *49*, 7516.
(46) Fivaz, R.; Mooser, E. Mobility of Charge Carriers in Semiconducting Layer Structures. *Phys. Rev.* **1967**, *163*, 743−755.
(47) Schmidt, E.; Sourisseau, C.; Meunier, G.; Levasseur, A. Amorphous Molybdenum Oxysulfide Thin Films and Their Physical Characterization. *Thin Solid Films* **1995**, *260*, 21−25.
(48) Radisavljevic, B.; Kis, A. Mobility Engineering and a Metal-Insulator Transition in Monolayer $MoS_2$. *Nat. Mater.* **2013**, *12*, 815−820.
(49) Ayari, A.; Cobas, E.; Ogundadegbe, O.; Fuhrer, M. S. Realization and Electrical Characterization of Ultrathin Crystals of Layered Transition-Metal Dichacogenides. *J. Appl. Phys.* **2007**, *101*, 014507-1−014507-5.


DOI: 10.1021/la504162u
*Langmuir* 2015, 31, 1196−1202

# SUPPORTING INFORMATION

## High turnover frequency of hydrogen evolution reaction on amorphous $MoS_2$ thin film directly grown by atomic layer deposition

Seokhee Shin,[†] Zhenyu Jin,[†] Do Hyun Kwon, Ranjith Bose and Yo-Sep Min*

Department of Chemical Engineering, Konkuk University, 120 Neungdong-Ro, Gwangjin-Gu, Seoul 143-701, Korea
e-mail: ysmin@konkuk.ac.kr

**Preparation of working electrode with catalyst:** After the ALD of $MoS_2$ on Au/Ti/Si substrate, the geometrical area of the catalytic film was defined with a Kapton tape as shown in Fig. S1. The specimen was connected to a metal wire using silver paste. During the electrochemical measurements, the defined area of the working electrode was immersed into the electrolyte solution.

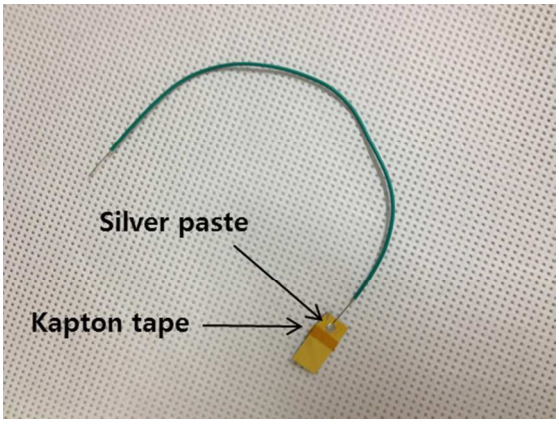


**Figure S1**. Picture of $MoS_2$/Au/Ti/Si working electrode of which the geometric area was defined to 1 $cm^2$ by a Kapton tape. The specimen was connected to a metal wire using silver paste.

**Ohmic potential drop (iR) correction:** The ohmic drop correction was performed with a series resistance ($R_s$) determined by electrochemical impedance measurement, according to the method given in Ref. S1. In our electrochemical setup, the series resistance may contain four components arising from the resistance in the wiring ($R_{wiring}$, e.g., electrode cables, alligator clips, Ag paste), the resistance in the Au substrate ($R_{gold}$), the solution resistance ($R_{sol}$) and the resistance due to the $MoS_2$ film itself ($R_{film}$). The electrochemical impedance measurements were performed at open circuit potential from 200 kHz to 50 mHz, using an AC amplitude of 25 mV. For all specimens, the series resistance was determined to be ~2.5 Ω by the real component of the impedance at high frequencies where the imaginary component is negligible, as shown in the Nyquist plot of Fig. S2. This reveals that the contribution of $R_{film}$ to the series resistance is negligible. Therefore the iR correction using the measured $R_s$ does not overestimate the HER activity. The experimental overpotential ($\eta_{exp}$) was corrected by subtracting the ohmic drop ($iR_s$) as the equation of $\eta_{corr} = \eta_{exp} - iR$.

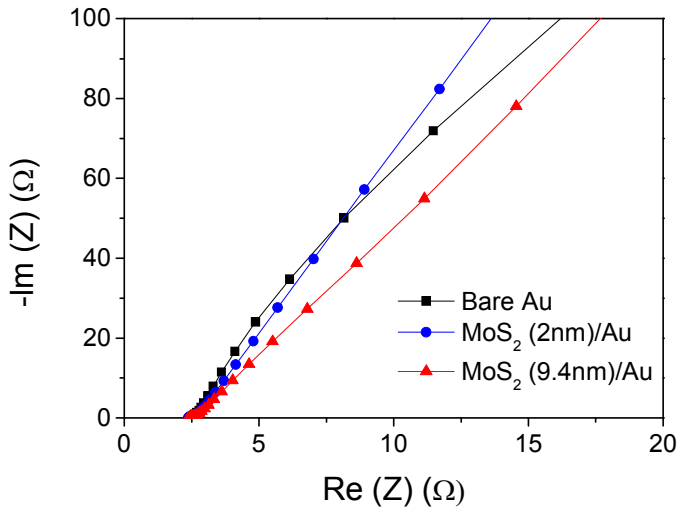


**Figure S2**. Nyquist plots of $MoS_2$ thin films and bare gold specimens performed at open circuit potential from 200 kHz to 50 mHz, using an AC amplitude of 25 mV. The series resistance was measured to be ~2.5 Ω for all specimens.

**Capacitance measurements:** Since the effective surface area of the catalyst film is linearly proportional to the double layer capacitance ($C_{dl}$), we performed cyclic voltammetry (CV) to obtain the values of $C_{dl}$ for the $MoS_2$ films and the bare Au specimen in a potential range of 0.1 ~ 0.2 V with various scan rates (20, 40, 60, 80, 100 mV/s), according to the method in the Ref. S2. The cathodic ($J_c$) and anodic ($J_a$) current densities of the cyclic voltammograms in Figs. S3 (a-c) should be mainly originated from the charging of the electric double layer, because there is no faradaic process in the voltage range. In Fig. S3d, the current density difference ($\Delta j$) of $J_c$ and $J_a$ at 0.15 V vs RHE was plotted against the scan rate and fitted to a linear line. The slope represents a doubling of the double layer capacitance. The double layer capacitance of the bare Au, $MoS_2$ (2 nm)/Au, and $MoS_2$ (9.4 nm)/Au specimens are 8, 45, and 152 $\mu F/cm^2$, respectively. Comparing the double layer capacitances of the two $MoS_2$ specimens, the thinner film has a $C_{dl}$ value 3.4 times smaller than the thicker film. This reveals that $MoS_2$ did not completely cover Au in the $MoS_2$ (2 nm)/Au specimen due to the ultrathin thickness.

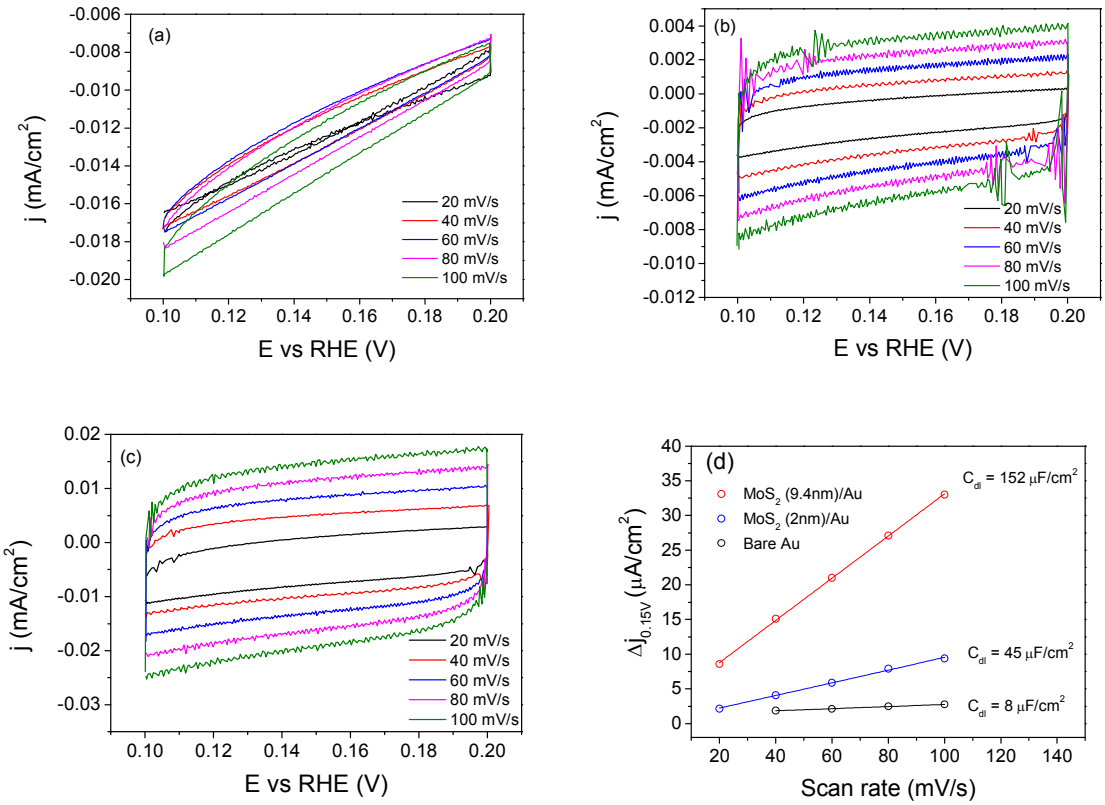


**Figure S3**. (a-c) Cyclic voltammograms in the range of 0.1 ~ 0.2 V vs RHE for the bare Au (a), $MoS_2$ (2 nm)/Au (b) and $MoS_2$ (9.4 nm)/Au (c) specimens. (d) The differences in current density ($\Delta j = j_a - j_c$) at 0.15 V vs RHE plotted against scan rate. The each plot was fitted to a linear line to determine the value of $C_{dl}$.

**Grazing incidence X-ray reflectivity (XRR):** For the $MoS_2$ film grown on a bare Si wafer, we performed low angle XRR measurement in the 2θ range of 0 ~ 2° in order to obtain the film density. The experimental data was fitted for the film to be 12.8 nm with a density of 2.9 g/cm$^3$ as shown in Fig. S4. The thickness determined by XRR roughly agrees with the thickness (11.5 nm) determined by spectroscopic ellipsometer with a Tauc-Lorentz dispersion function.[S3] In addition, the density of the film reveals that the film is less dense in comparison to the crystalline $MoS_2$, due to the amorphous nature of the film grown at 100 °C.

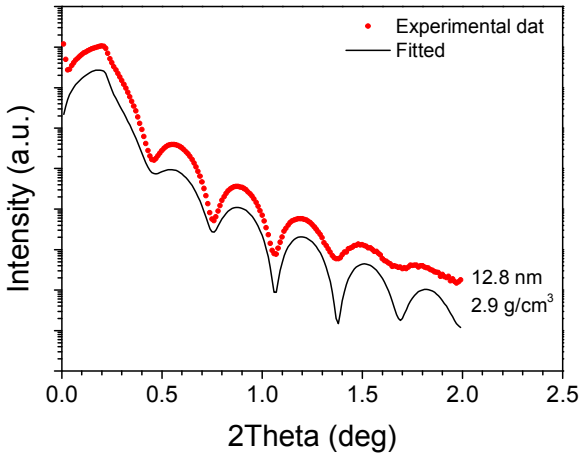


**Figure S4**. Low angle XRR data and its fitted curve for $MoS_2$/Si specimen.

**Scanning electron microscopy (SEM) images:** The high resolution SEM images were taken on the $MoS_2$ film grown on Au. For these images, any metal, which is generally coated on an insulating specimen to avoid the charging effect by electron beam, was not coated on the specimen, because the $MoS_2$ film is considerably conducting (Fig. 5). For the $MoS_2$ (2 nm)/Au, the grains of Au are clearly visible due to the ultrathin thickness. However the $MoS_2$ (9.4 nm)/Au specimen shows that the grains and their boundaries are covered by the film, even though the surface is still rough.

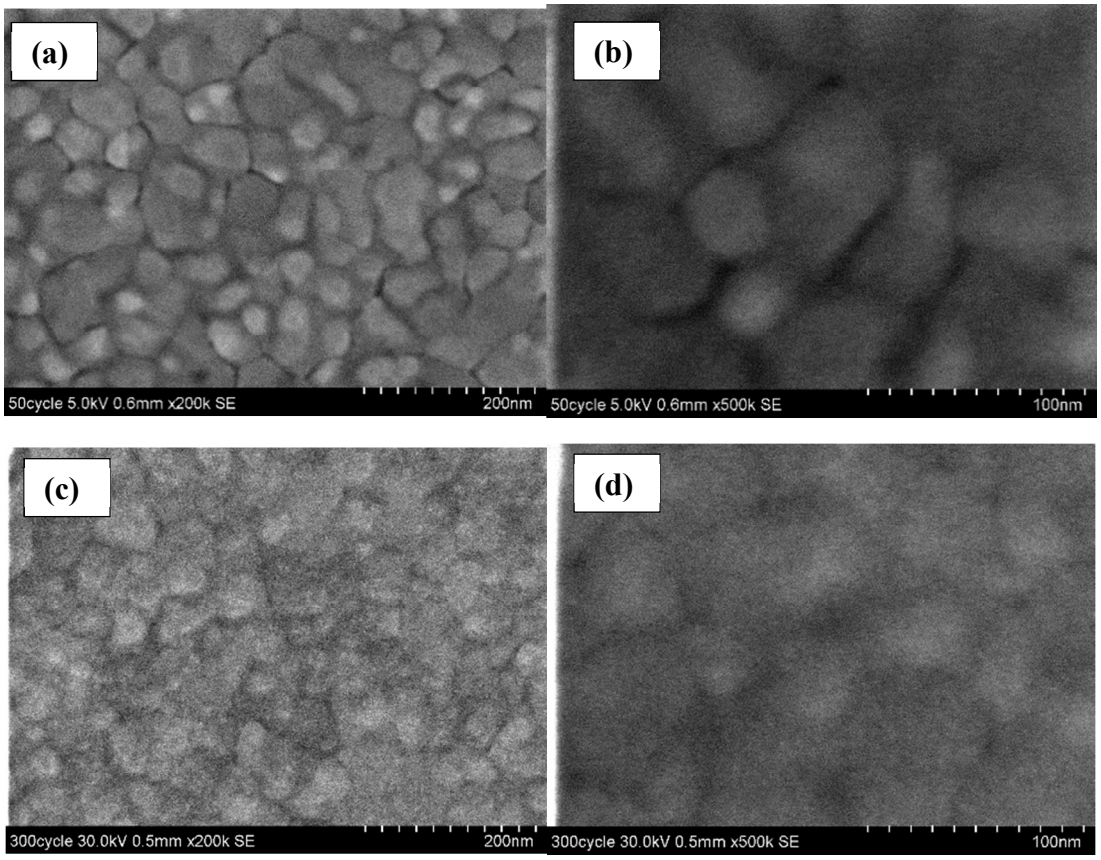


**Figure S5**. SEM images of $MoS_2$ (2 nm)/Au (a - b) and $MoS_2$ (9.4 nm)/Au (c - d).

**Stability test of ALD-$MoS_2$ catalyst:** For the stability test of the ALD-$MoS_2$/Au catalyst, the cyclic voltammetry (CV) was repeated for 1000 cycles between 0.205 ~ -0.195 V vs. RHE in 0.5 M $H_2SO_4$. There is a significant loss of activity after 1000 CV cycling.

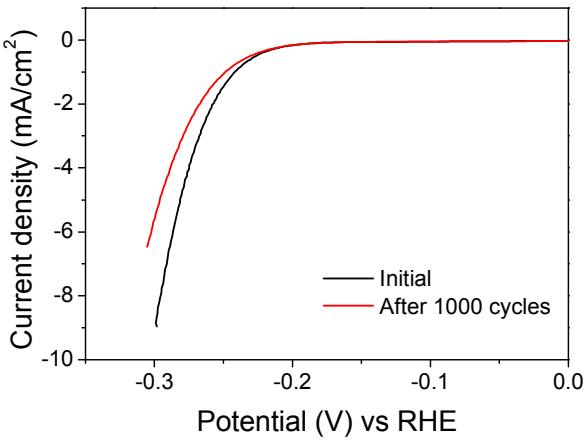


**Figure S6**. Stability of ALD-$MoS_2$/Au catalyst before and after 1000 CV cycling.

References

(S1) Chen, Z.; Cummins, D.; Reinecke, B. N.; Clark, E.; Sunkara, M. K; Jaramillo, T. F. *Nano Lett*. **2011**, 11, 4168.

(S2) Lukowski, M. A.; Daniel, A. S.; Meng, F.; Forticaux, A.; Li, L.; Jin, S. *J. Am. Chem. Soc.* **2013**, 135, 10274.

(S3) Yim, C.; O'Brien, M.; McEvoy, N.; Winters, S.; Mirza, I.; Lunney, J. G.; Duesberg, G. S. *Appl. Phys. Lett.* **2014**, 104, 103114.